Open access • Journal Article • DOI:10.1108/13552540610707013

Residual stresses in selective laser sintering and selective laser melting

Peter Mercelis, Jean-Pierre Kruth

Institutions: Katholieke Universiteit Leuven

Published on: 01 Jan 2006 - Rapid Prototyping Journal (Emerald Group Publishing Limited)

Topics: Residual stress, Selective laser sintering, Selective laser melting and Laser scanning

Residual stresses in selective laser sintering and selective laser melting

Peter Mercelis and Jean-Pierre Kruth
Division PMA, Department of Mechanical Engineering, University of Leuven, Leuven, Belgium

Abstract
Purpose – This paper presents an investigation into residual stresses in selective laser sintering (SLS) and selective laser melting (SLM), aiming at a better understanding of this phenomenon.
Design/methodology/approach – First, the origin of residual stresses is explored and a simple theoretical model is developed to predict residual stress distributions. Next, experimental methods are used to measure the residual stress profiles in a set of test samples produced with different process parameters.
Findings – Residual stresses are found to be very large in SLM parts. In general, the residual stress profile consists of two zones of large tensile stresses at the top and bottom of the part, and a large zone of intermediate compressive stress in between. The most important parameters determining the magnitude and shape of the residual stress profiles are the material properties, the sample and substrate height, the laser scanning strategy and the heating conditions.
Research limitations/implications – All experiments were conducted on parts produced from stainless steel powder (316L) and quantitative results cannot be simply extrapolated to other materials. However, most qualitative results can still be generalized.
Originality/value – This paper can serve as an aid in understanding the importance of residual stresses in SLS/SLM and other additive manufacturing processes involving a localized heat input. Some of the conclusions can be used to avoid problems associated with residual stresses.

Keywords Sintering, Lasers, Stress (materials)

Paper type Research paper

Introduction

Selective laser sintering (SLS) and selective laser melting (SLM) are two production technologies offering great advantages and opportunities compared to traditional material removal techniques (Kruth *et al.*, 2003, 2004). However, the residual stresses that arise in the parts being produced impose some serious limitations to the practical use, since they introduce part deformations and/or micro cracks. Moreover, large residual stresses can limit the load resistance of the parts compared to a stress free state.

In the field of Laser Engineered Net Shaping, a lot of effort has been done to measure, predict and control residual stresses (Vasinonta *et al.*, 2000; Aggarangsi and Beuth, 2003). Whereas researchers mainly focussed on the stresses in the growth-direction at the substrate-part connection, the current research will focus on the stresses perpendicular to the build direction, and their variation along the build direction.

In order to investigate the residual stresses, the origin of the stresses is firstly explained. Next, a simple theoretical model is presented to predict the basic residual stress distribution. Using an experimental procedure, residual stress profiles are then measured in a set of test samples having different kinds of process parameters. Thus, the effect of the process parameters on the residual stress can be concluded. Finally, some guidelines are presented to reduce the residual stress in SLS and SLM.

The difference between SLS and SLM concerns the binding mechanism that occurs between the powder particles (Kruth *et al.*, 2004). In SLS, either a combination of a low melting binder and high melting structural material is used - called liquid phase sintering (LPS) or the powder particles are just partially molten. In case of LPS, a post treatment is generally necessary to enhance the mechanical properties and to increase the part's density. In SLM, the powder particles are fully molten. Since the border between SLS and SLM is rather vague, the stress inducing mechanisms are explained generally for the case of SLM. In the case of partial melting without infiltration, the same stress inducing mechanisms will occur. On the other hand, in the case of the LPS mechanism, the furnace cycle that is used to infiltrate the parts, will result in stress relaxation, so the resulting parts can be expected to be stress free.

The origin of residual stresses

Residual stresses are stresses that remain inside a material, when it has reached equilibrium with its environment. Residual stresses are generally classified according to the scale at which they occur (Withers and Bhadeshia, 2001). This investigation includes only

The current issue and full text archive of this journal is available at
www.emeraldinsight.com/1355-2546.htm

Rapid Prototyping Journal
12/5 (2006) 254–265
 [ISSN 1355-2546]
[DOI 10.1108/13552540610707013]

This research was funded by the IAP project P5-08 of the Belgian Federal Science Policy and the GOA/2002/06 project from KU Leuven.
Received: 1 January 2006
Revised: 1 March 2006
Accepted: 23 June 2006

type I residual stresses, which vary over large distances, namely the dimensions of the part. These macro stresses can result in large deformations of the part. Type II and type III residual stresses, which occur due to different phases in the material and due to dislocations at atomic scale, are not considered in this study, since they are of less importance for the material's strength. Moreover, the measurement resolution of most test methods is not small enough to measure type II and type III residual stresses.

Residual stresses are not always disadvantageous, e.g. glass plates are many times rapidly cooled to introduce compressive stress in the surface area of the plate, thus increasing the overall loading resistance and preventing crack growth at the surface. However, in most cases, residual stresses are unwanted, since they result in deformations from the intended shape. Moreover, tensile pre-stress adds to the stresses caused by external loading, thus reducing the strength of the parts and favoring propagation of cracks from the surface.

Each production process introduces some amount of residual stress (Withers and Bhadeshia, 2001). However, the amount of residual stress that is introduced varies a lot among different production processes. Laser based processes (laser welding, SLM, etc.) are known to introduce large amounts of residual stress, due to the large thermal gradients which are inherently present in the processes. In case of laser bending, these stresses are, e.g. used to deform sheet metal plates to a desired shape. Two mechanisms can be distinguished which cause residual stresses.

The first mechanism introducing residual stress is called the temperature gradient mechanism (TGM, Figure 1). It results from the large thermal gradients that occur around the laser spot. The TGM mechanism is commonly used for laser bending of sheets along straight lines. Owing to the rapid heating of the upper surface by the laser beam and the rather slow heat conduction, a steep temperature gradient develops. The material strength simultaneously reduces due to the temperature rise. Since the expansion of the heated top layer is restricted by the underlying material, elastic compressive strains are induced. When the material's yield strength is reached, the top layer will be plastically compressed. In absence of mechanical constraints, a counter bending away from the laser beam would be perceived. During cooling the plastically compressed upper layers start shrinking and a bending angle towards the laser beam develops. This mechanism is also present in SLS and SLM, where the underlying layers inhibit the expansion of the heated top layers. It is important to notice that this mechanism does not require the material to be molten.

A second mechanism that induces residual stresses is the cool-down phase of the molten top layers (in SLM). The latter tend to shrink due to the thermal contraction. This deformation is again inhibited by the underlying material, thus introducing tensile stress in the added top layer and compressive stress below.

Figure 1 TGM inducing residual stress

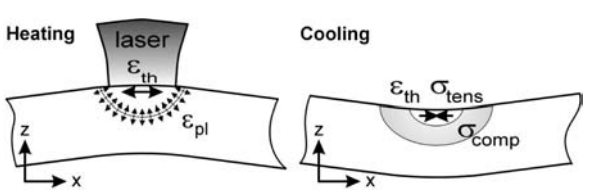

Simplified theoretical model

To get an idea of the residual stress profiles that would be found in SLM samples, a simplified theoretical model was developed. Assume that a part is being built on top of a base plate with height h_b. The part that was built so far has height h_p and the layer thickness is t (Figure 2). This simple theoretical model assumes that:

- the base plate and the part being built are at room temperature;
- the upper layer induces stress due to its shrinkage ($\alpha\Delta T$); the tensile stress is equal to the material's yield strength σ (since a strain of $\alpha\Delta T$ would result in a stress much larger than the material's yield strength);
- the stress σ_{xx} is independent of the y coordinate, i.e. the variation of the normal stress across the part's width is neglected;
- the general beam theory is valid; and
- no external forces are applied to the combination part-base plate.

At each moment, the equilibria of force equation (1) and moment equation (2) need to be obeyed, since there are no external forces acting on the system:

$$\int \sigma_{xx}(z)\mathrm{d}z = 0 \tag{1}$$

$$\int \sigma_{xx}(z)z\mathrm{d}z = 0 \tag{2}$$

Owing to the continuity of the deformation at the border between the base plate, following strain profile is assumed over the combination base plate-part:

$$\epsilon_{xx}(z) = az + b \tag{3}$$

Owing to the different stiffness of the base plate and the part material, this deformation results in different stress levels; the stress profile reveals a jump at the border between the base plate and the part. Suppose that m represents the ratio of base plate stiffness to the part's stiffness:

$$m = \frac{E_{\text{base}}}{E_{\text{part}}} \tag{4}$$

Using this assumption, the equilibrium conditions can be rewritten as:

Figure 2 Simplified theoretical model of the SLM process

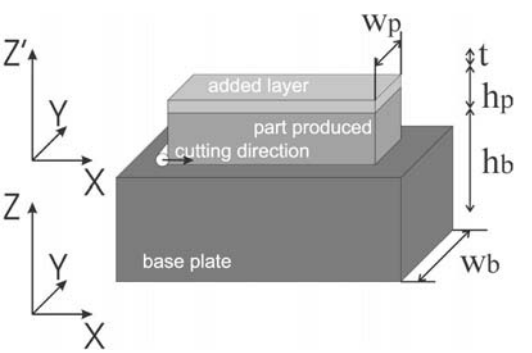

$$\int_0^{h_b} m(az+b)\mathrm{d}z+\int_{h_b}^{h_b+h_p}(az+b)\mathrm{d}z+\int_{h_b+h_p}^{h_b+h_p+t}\bar{\sigma}\mathrm{d}z=0 \quad (5)$$

$$\int_0^{h_b} m(az+b)z\mathrm{d}z+\int_{h_b}^{h_b+h_p}(az+b)z\mathrm{d}z+\int_{h_b+h_p}^{h_b+h_p+t}\bar{\sigma}z\mathrm{d}z=0 \quad (6)$$

From equations (5) and (6), the coefficients a and b can be derived:

$$a=-6\bar{\sigma}t\frac{(2mh_bh_p+mh_bh_pt+h_p^2+h_pt+mh_b^2)}{(4mh_b^3h_p+h_p^4+m^2h_b^4+6mh_b^2h_s^2+4mh_bh_p^3)} \quad (7)$$

$$b=\bar{\sigma}t\frac{(2mh_b^3+6h_pmh_b^2+3mh_b^2t+6h_bh_p^2+6h_bh_pt+2h_p^3+3h_p^2t)}{(4mh_b^3h_p+h_p^4+m^2h_b^4+6mh_b^2h_s^2+4mh_bh_p^3)} \quad (8)$$

Equations (5) and (6) assume that the part and the base plate are equally wide. Usually the base plate is wider than the part. Including the widths of the part and the base plate in the equations would result in a different m factor: $m=E_{\mathrm{base}}w_{\mathrm{base}}/E_{\mathrm{part}}w_{\mathrm{part}}$. The influence of a wider base plate can thus be simulated by increasing the E modulus of the base plate.

After the production, the parts produced are generally removed from the base plate. To simulate this, a relaxation stress must be added to the stress profile calculated in the part. This relaxation stress has a linear profile ($z'=z$-h_b, Figure 2):

$$\sigma_{\mathrm{relaxation}}(z')=cz'+d \quad (9)$$

The constant part of the relaxation stress corresponds to a uniform shrinkage of the part that is being removed from the base plate. The linear part results in a curvature of the part. The coefficients c and d can be determined by recalculating the equilibrium conditions for the produced part (with h_c the height of the part in the new coordinate system X, Y, Z'):

$$c=-6\frac{-2\int_0^{h_c}z'\sigma(z')\mathrm{d}z'+h_c\int_0^{h_c}\sigma(z')\mathrm{d}z'}{h_c^3} \quad (10)$$

$$d=2h_c\frac{\int_0^{h_c}\sigma(z')\mathrm{d}z'-3h_c\int_0^{h_c}z'\sigma(z')\mathrm{d}z'}{h_c^2} \quad (11)$$

Theoretical residual stress profiles

When a layer is added to the base plate, it induces a compressive stress in the upper part of the base plate and a tensile stress in the lower part. When successive layers are added on top, each layer induces a certain stress profile in the base plate, but also in the underlying solidified layers, thus reducing the initial tensile stress present in these layers.

Figure 3 shows the resulting stress profile in the part and baseplate, after 50 layers (properties: base plate thickness = 20 mm, $E_{\mathrm{base}}=210$ GPa, $E_{\mathrm{part}}=110$ GPa, $t=50\,\mu$m, $\sigma=300$ MPa). It can be seen that the stress at the last added layer equals the yield stress of the material.

When the part is removed from the base plate, the stress state in the part is drastically changed; due to the relaxation, the resulting stress in the part will be much lower. The constant part of the relaxation stress corresponds to the shrinkage of the part, whereas the linear part of the relaxation stress corresponds to the bending deformation. Figure 4 shows the relaxation principle and the resulting stress in the part.

Figure 3 Residual stress in the part and the base plate

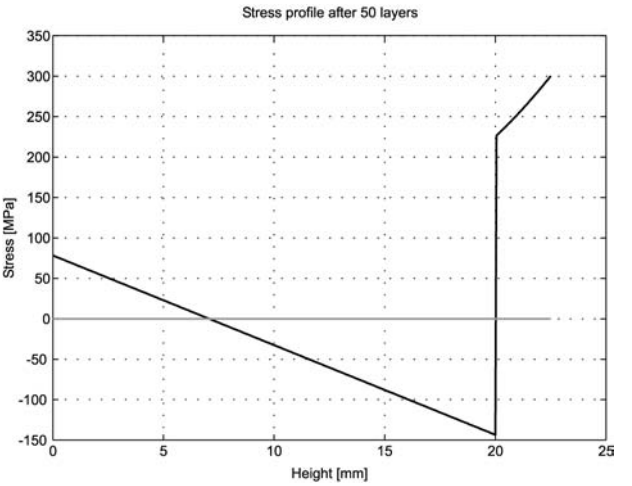

Influence of number of layers, base plate geometry and material properties

Number of layers

Figure 5 shows the influence of the number of layers on the residual stress profile. Before part removal, the stress in the part equals the yield strength at the top. However, when the number of layers keeps increasing, compressive stresses occur at the bottom of the part. It can also be seen that the stresses in the base plate become very large, so plastic deformation of the base plate could occur. However, this behaviour is not included in the model. After part removal, a more or less symmetrical stress profile remains in the part. At the top and bottom of the part, tensile residual stress remains, with a zone of compressive stress in between. The tensile residual stress is somewhat larger at the bottom than at the top surface.

Figure 6 shows the influence of the number of layers on the relaxation stresses. It can be seen that the constant part, which relates to the shrinkage in X direction, is reduced by adding more layers, while the linear part is increased. However, one should not conclude that this would increase the part's bending deformation, since the surface moment of inertia increases with the number of layers (according to h^3).

Base plate geometry

Since the model assumes that the general beam bending theory is valid, the width of the base plate can be combined with its E modulus to represent the stiffness. The base plate height, however, must be treated separately. Figure 7 shows the influence of the base plate height on the stress profiles. According to this simple theoretical model, the height of the base plate has a clear influence on the residual stress distribution. Before part removal, a higher height results in a lower stress level in the base plate itself and a more uniform stress level in the part. This means that a thick base plate results in a smaller deformation due to part removal, compared to a thin base plate. Since almost all stress is released by a uniform shrinkage, only little residual stress remains in the part after removal. Figure 8 shows the influence of the base plate height on the relaxation stress components.

Material properties

Figure 9 shows the influence of the material's yield strength on the residual stress being developed. The higher the yield

Figure 4 Relaxation of the residual stress and resulting stress in the part

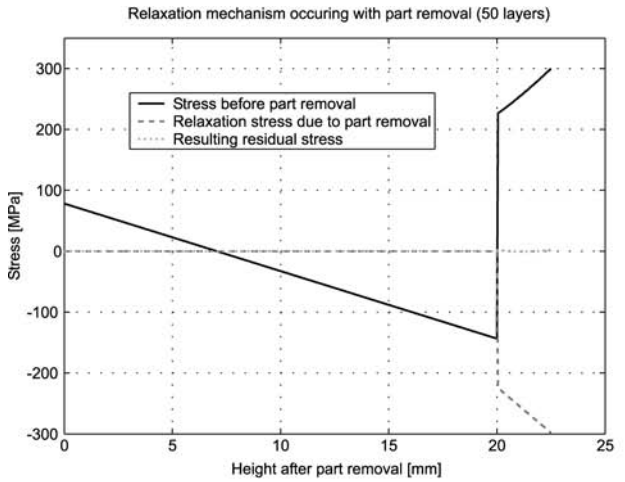

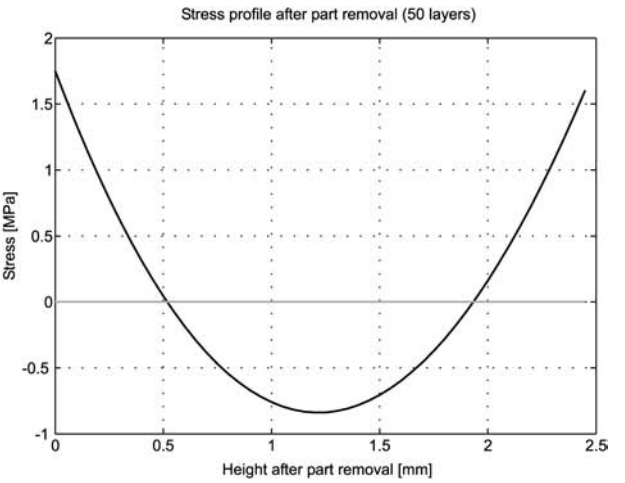

Figure 5 Influence of the number of layers on the residual stress profile

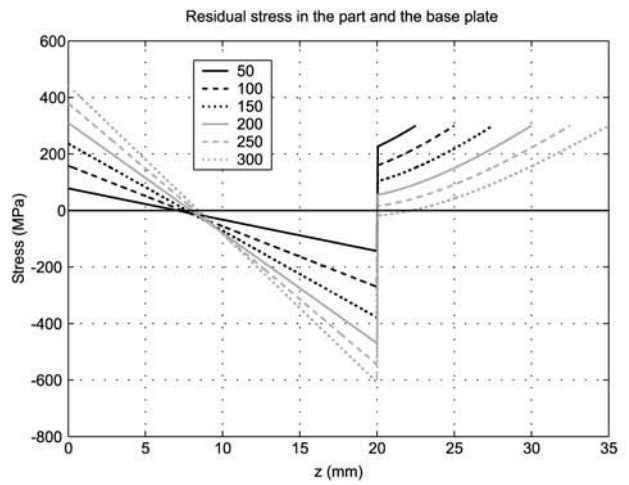

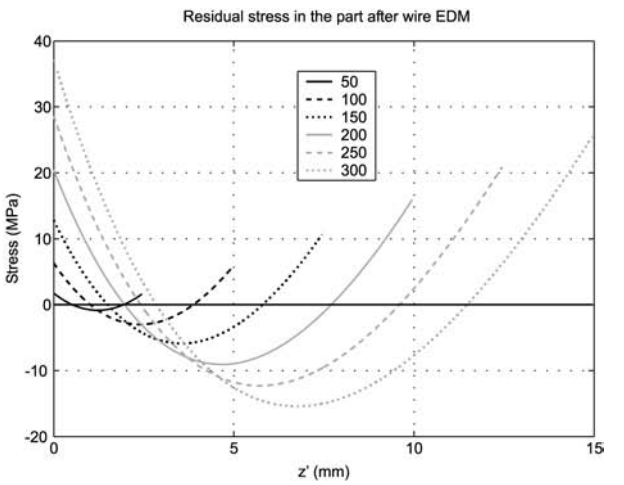

Figure 6 Influence of the number of layers on the relaxation stress

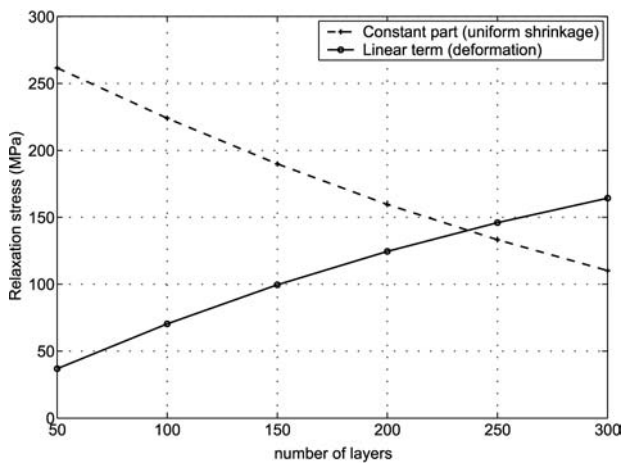

strength, the higher the stresses being developed. The stresses after part removal are also larger.

Conclusions

- Stress profiles before removal consist of a large zone of tensile stress at the upper zone of the part being built. The maximum stress is reached at the surface of the part (equal to the yield stress). The stress reduces with decreasing Z values. The lower part of the base plate is under tensile stress, the upper part is under compressive stress.
- Part removal drastically reduces the residual stresses which are present in the part; the residual stress relaxes by a uniform shrinkage and a bending deformation. The residual stress after removal consists of a zone of tensile stress at the upper and lower zone of the part and a compressive stress zone in between. The stresses after part removal are much smaller than before part removal.

Figure 7 Influence of the base plate height on the residual stress profile

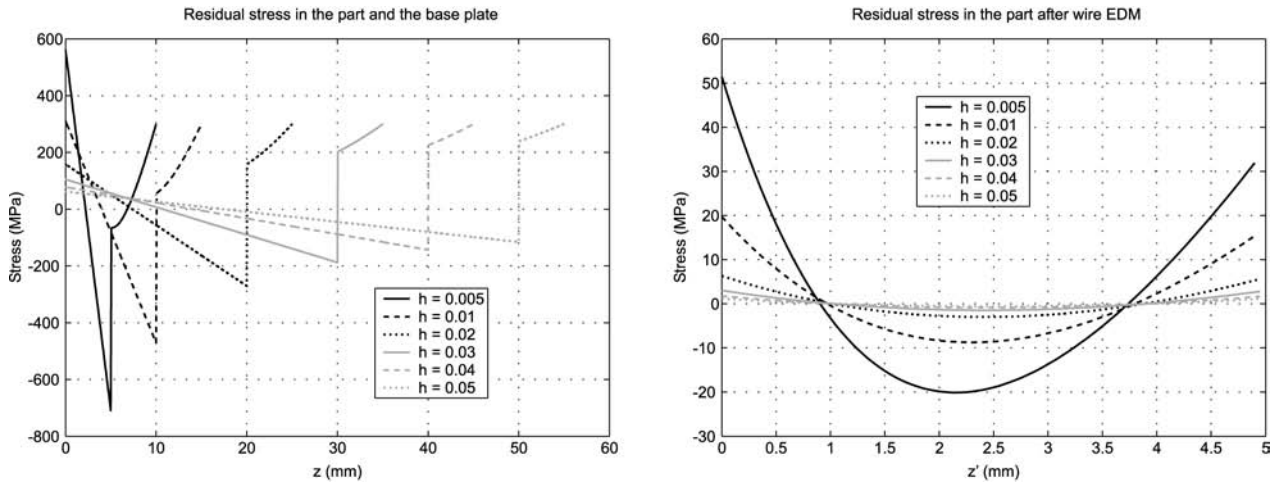

Figure 8 Influence of the base plate height on the relaxation stress components

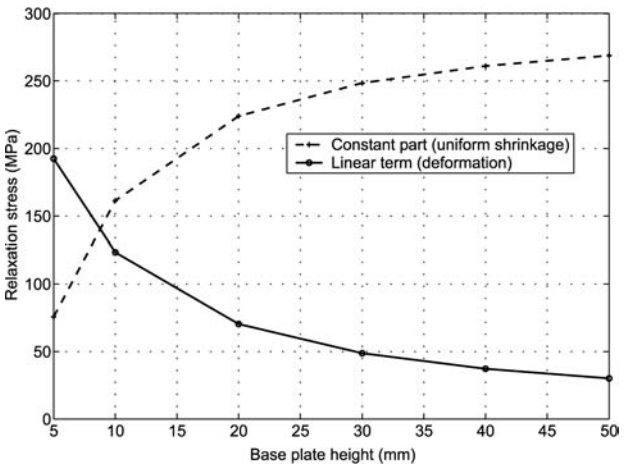

Figure 9 Influence of the materials yield strength on the residual stress profile

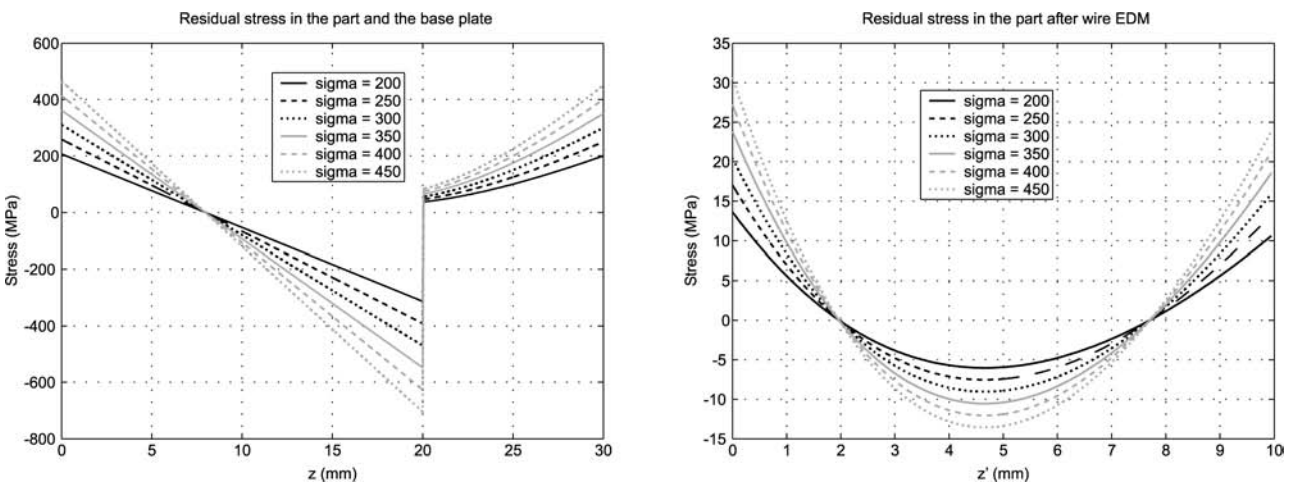

- The more layers are added, the larger the final residual stress will be. The shrinkage along the X axis will reduce when the amount of layers increases.
- The thicker the base plate, the smaller the resulting residual stresses will be (for a fixed part thickness). A very thick base plate results in a large shrinkage in X direction, while the bending deformation becomes smaller. A thin base plate height results in high residual stresses in the part and in a high bending deformation.
- The higher the yield strength of the added material, the higher the resulting residual stresses.

Experimental measurement of residual stress: the Crack compliance method

In order to measure the residual stresses in the parts, a novel experimental model is used, based on measurement of the part's deformation when the stresses are relieved. The method is called the "Crack Compliance Method" (CCM) (Prime, 1999; Nowell *et al.*, 2000). Compared with "traditional" test methods like X-ray diffraction or hole drilling, this method has the advantage that trough-thickness measurements can be performed in a simple and cheap way (Schindler, 2000). The method will be shortly explained first, without discussing the mathematical implementation in detail.

Figure 10 shows a sample in which an unknown residual stress distribution $\sigma_{xx}(z)$ is present. This stress distribution is supposed to be independent from the Y coordinate. One or more strain gauges are connected to the sample's surface at known positions. Next, the part is cut in subsequent small steps using wire electric discharge machining (EDM). After each cutting step, the strain is measured at each strain gauge position.

Suppose that the unknown stress distribution can be written as a series expansion of functions $P_j(z)$.

$$\sigma_{xx}(z) = \sum_{j=1}^{n} A_j P_j(z) = [P]\{A\} \tag{12}$$

The set of basic functions $P_j(z)$ can be polynomials, Fourier series, etc. Legendre polynomials are generally chosen, since these polynomials (from order 2 on) automatically obey the equilibrium conditions of force and moment. For each basic function $P_j(z)$ we can now calculate the strain profiles that would be measured at the strain gauge locations, if this basic function was the actual residual stress profile. These calculations are generally performed using a finite element method[1]. The calculated strains, belonging to each of the basic functions, are referred to as "compliances" $C_j(d_i)$. Using the superposition principle, the total strain due to the sum of all the basic functions can be written as:

Figure 10 Schematic representation of test sample

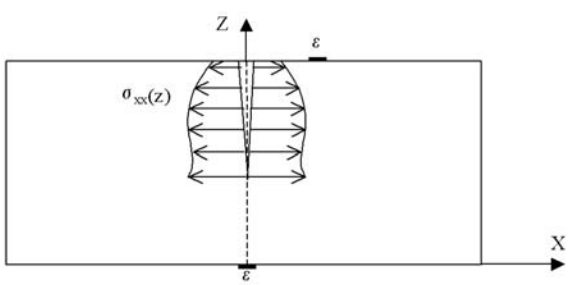

$$\epsilon_{xx}(z) = \sum_{j=1}^{n} A_j C_j(z) = [C]\{A\} \tag{13}$$

From equation (13), the coefficients A_j can be calculated using a least-squares fitting algorithm:

$$\{A\} = ([C^{\mathrm{T}}][C])^{-1}[C]^{\mathrm{T}}\{\epsilon_{\mathrm{measured}}\} \tag{14}$$

Substitution of the coefficients $[A]$ in equation (12) results in the residual stress profile.

Figure 11 shows the compliance functions that were calculated for the selected top face and back face strain gauge positions.

In practise, the strains are measured at two locations, while the parts are being cut by wire-EDM. Figure 12 shows the practical setup.

Experimental results

Test of the CCM method

In order to evaluate the suitability of the Crack compliance method to do residual stress tests on SLM samples, and to check the FEM model being used, some initial experiments were performed on samples with a know residual stress distribution.

A first tests performs a stress measurement on an aluminium sample that was heated up to 200°C for 1 h and cooled in air, to remove all residual stresses. Figure 13 shows the stress distribution that was calculated from the strain measurements. As it can be seen, the stress level of 0 MPa lies within the two sigma uncertainty bound (95 per cent confidence limit) at most points.

Using a four point bending setup some test samples were produced, having a known stress distribution. The four point bending test ensures a constant bending moment between the two middle contact points. The samples were bent until plastic deformation occurs at the upper and lower zones of the parts. After removing the force, a new equilibrium is formed, that can be calculated from the recorded force values and the yield strength. Figure 14 shows the calculated stress profile for one of the test samples. The stress distribution that is calculated this way, assumes that the samples are bent according to the general beam bending theory. It also assumes a perfect elastic-plastic behaviour of the material, with a clear yield strength; in reality the real stress profile could be slightly different, but the general tendencies are assumed to be correct.

Figure 15 shows the stress profile that is calculated from the measured strains. It can be seen that the calculated stress distribution matches the "known" stress profile rather well. However, at some points large deviations occur.

Figure 16 shows the calculated stress distribution for a second test sample. In this case, the deviations are much larger. This is due to the steepness of the "real" stress profile, which cannot be fit accurately with the set of Legendre polynomials that is being used. This is shown in Figure 17 which shows the optimal fit of the "real" stress profile using the Legendre polynomials up to order 7. In order to fit these sharp peaks accurately, higher order polynomials are necessary. When sharp peaks are expected in a residual stress profile, the Legendre polynomials are therefore not the

Figure 11 Top face (left) and back face (right) compliance functions for 2nd-9th order Legendre polynomials

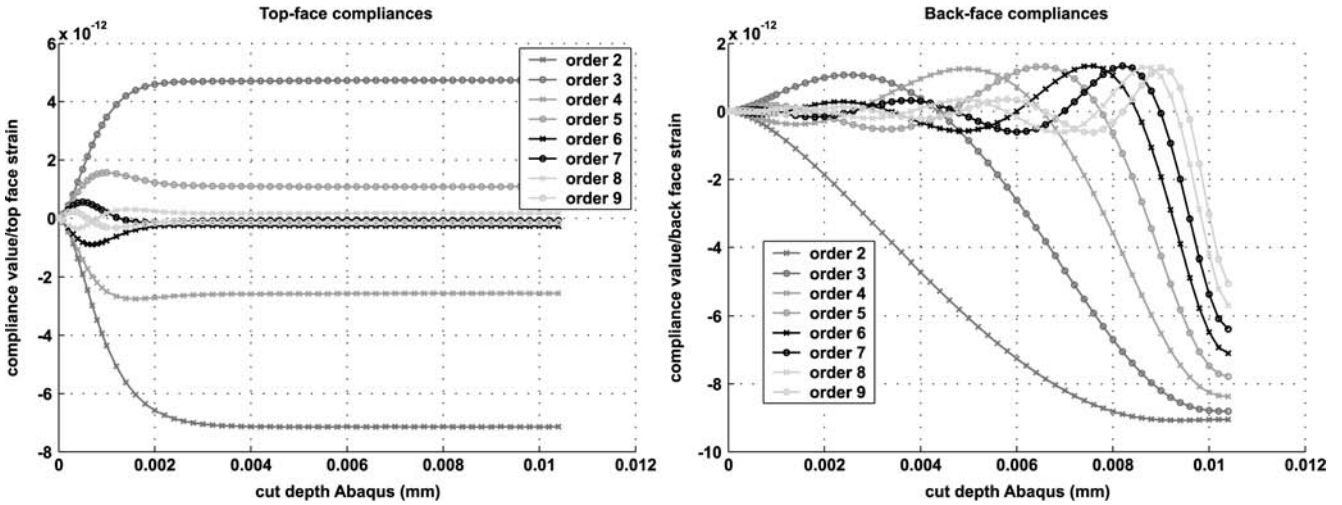

Figure 12 Practical setup of the CCM method

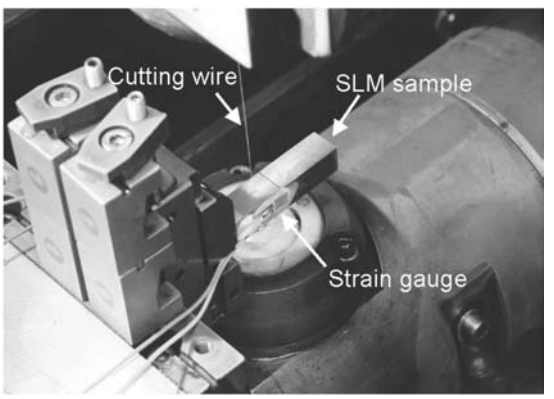

Figure 13 Calculated stress distribution in a stress free Al test sample

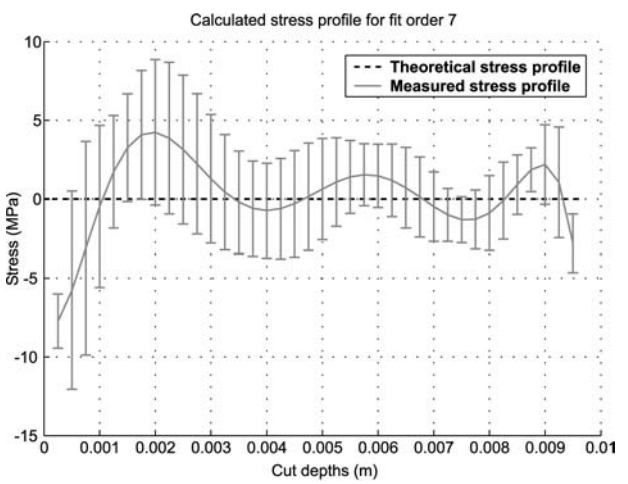

ideal ones and other types of basic functions are favorable. However, from the theoretical model there is no reason to expect sharp peaks in the residual stress profiles, thus the Legendre polynomials with their inherent force and moment equilibrium were used.

Description of test samples

Table I summarizes the most important test parameters of the test samples that were all built on a concept laser M3 linear machine. All test samples were produced from a standard stainless steel powder (grade 316L). The parts were built on top of a 15 mm thick stainless steel substrate plate.

Influence of the exposure strategy

The exposure strategy of the laser beam highly influences the thermal gradients which occur in the parts being produced. To test the influence of the exposure strategy on the residual stresses, a set of test samples was made using different scanning strategies. Figure 18 shows the different exposure strategies that were used.

The "line Y" part is scanned along the Y axis and is thus also referred to as "short track" scanning, while the "line X" part will be named "long track" scanning. To test the influence of the sector scanning, two different sector sizes were used: 5 by 5 mm and 10 by 10 mm. The position of the islands is shifted in X and Y direction between successive layers. The sector scanned parts discussed in this paragraph are all scanned according to a certain patented pattern, which minimizes the thermal influence of previous scanned sectors on the next scanned sector. The influence of the sector scanning order is investigated in the next paragraph.

Figure 19 shows the stress distributions that were measured for the exposure strategies. Some important conclusions can be derived:

- all stress profiles correspond to the general tendency of a small zone with high tensile stresses at the top of the part, followed by broad zone of compressive stress and again a small zone of tensile residual stress;
- there is a clear difference between "short track" scanning and "long track" scanning: scanning along the Y direction results in the largest values for σ_{xx}, while scanning along the X direction results in the smallest σ_{xx} values;
- division of the part surface in smaller sectors yields an intermediate stress level; the top layer stress lies between the stress resulting from "long" and "short" scanning of the whole part surface; and
- there is no significant difference in the resulting stress profile between 5 and 10 mm sector size.

Figure 14 Calculated stress distribution in bent test sample 1

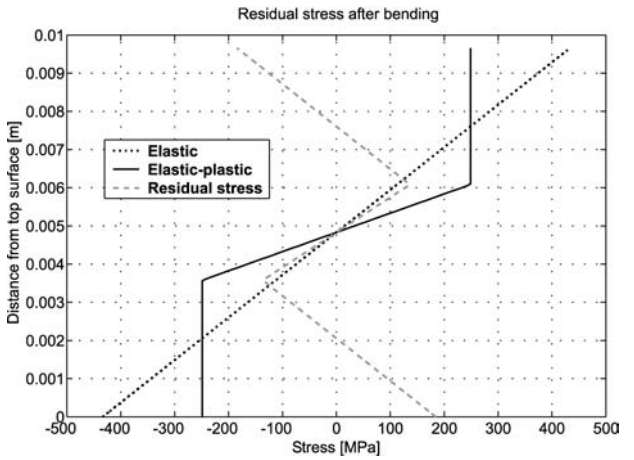

Figure 15 Calculated and measured stress distribution in bent test sample 1

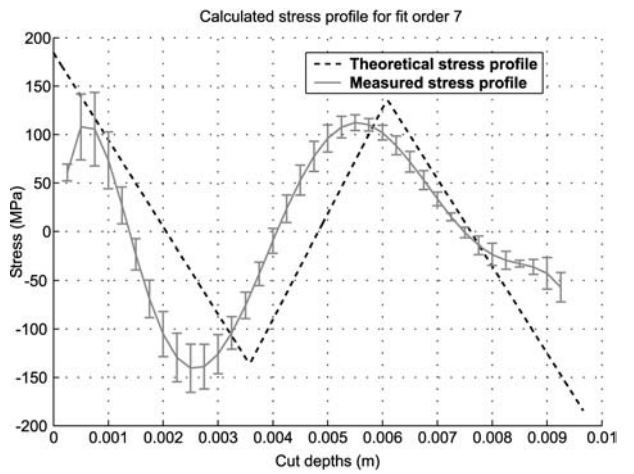

Figure 16 Calculated and measured stress distribution in bent test sample 2

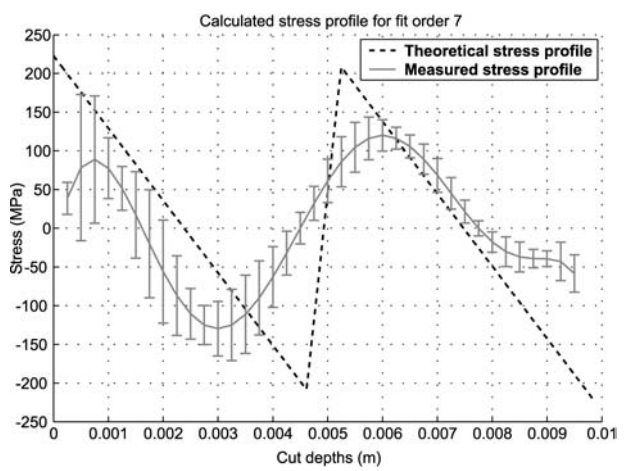

Figure 17 Optimal fit of the real stress profile of test sample 2 using Legendre polynomials up to order 7

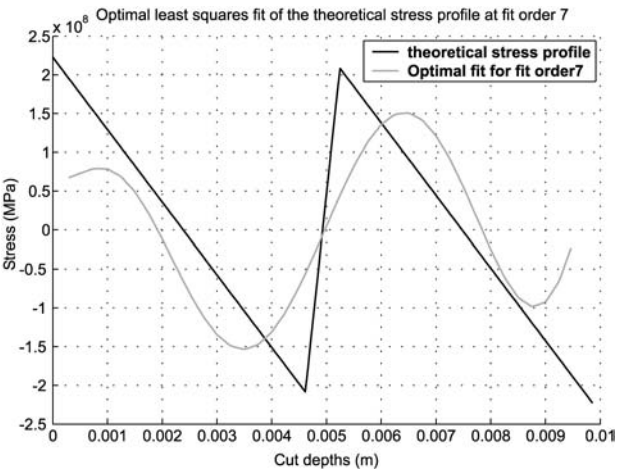

Table I Parameters used for the production of all test samples

Length	50 mm
Width	10 mm
Height	10.5 mm
Laser power	100 W
Scanning speed	400 mm/s
Scan spacing	140 μm
Layer thickness	30 μm

Figure 18 Different exposure strategies

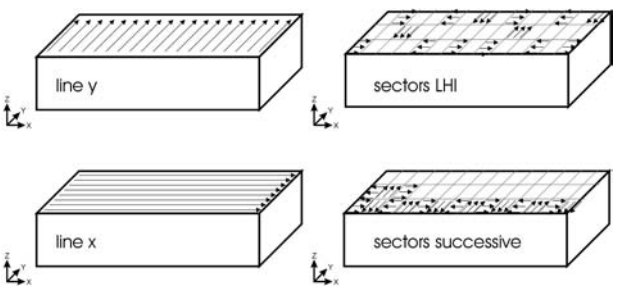

Figure 19 Measured stress distributions for different exposure strategies

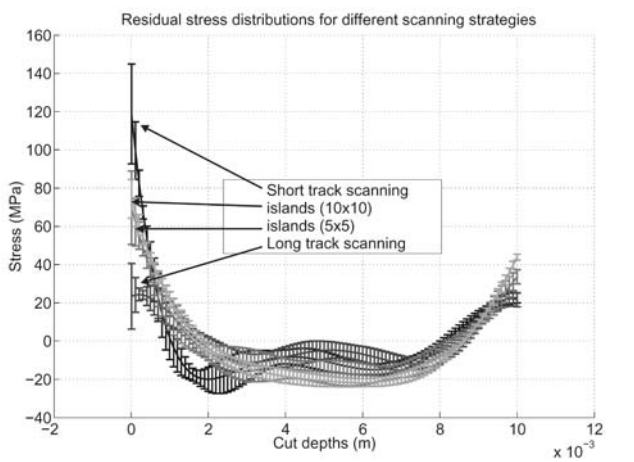

A possible explanation for the reduction of the maximal stress level in case of sector scanning, is the fact that the stress at the borders of each individual sector -that has no neighbouring sectors yet -is zero, since no material exhibits its contraction at the sector borders (Figure 20). When more sectors are added, neighbouring sectors are connected and the stress level also rises at the sector borders. However, the overall stress level will be still be lower than the maximum stress level in case of simple line scanning in the perpendicular direction.

Influence of the sector scanning order

Knowing that a subdivision of the part surface can reduce the largest tensile stresses that occur in the upper layers of the parts, the question remains how to expose these sectors. There are number of ways to do so. Three different exposure orders were tested in the investigation, all with the same sector size (3-3 mm):

1 scanning of the sectors along the width of the part;
2 scanning the sectors along the length of the part; and
3 scanning the sectors in a randomized order, minimizing the mutual thermal influence of the different sectors.

Since the exposure order of the sector influences the thermal gradients that occur, it also affects the level of residual stress in the parts. Figure 21 shows the difference between the two first exposure orders. It can be seen that scanning the sectors along the width of the part yields a larger σ_{xx} value at the top of the part, than scanning along the part's length. This is no surprise, since the exposure order along the part width corresponds to the "short track" scanning strategy, if the sector size goes to zero. The stress level in case of the randomized scanning order was comparable to the stress level when scanning along the length of the part (red curve in Figure 21), however, a bad top face strain reading resulted in a high uncertainty border.

Post scanning of the produced parts

To simulate a stress reducing heat treatment, post scanning of the part surface was investigated. After the normal exposure of each layer, the same layer was exposed again with the laser, at a lower energy level. Four parts were tested, with a post scanning energy of 10, 33, 50 and 100 per cent of the normal layer energy,

Figure 20 Sector scanning mechanism leading zero normal stress the first sector borders

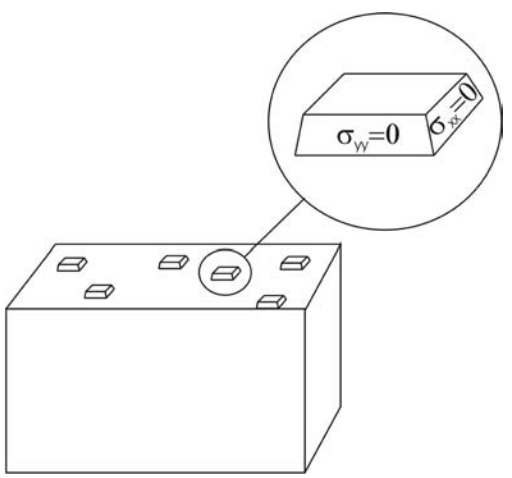

Figure 21 Measured stress distributions for different sector exposure orders

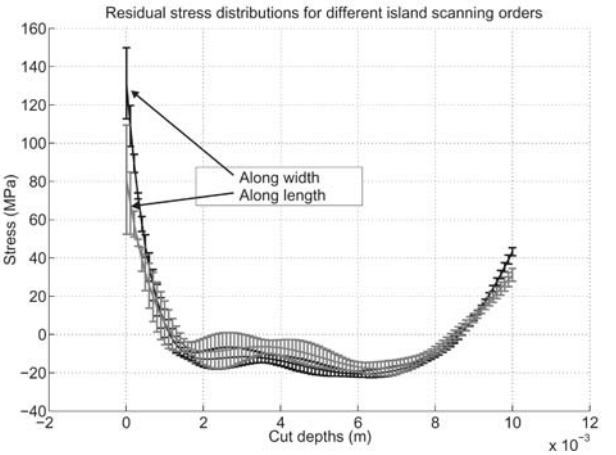

by increasing the scan speed accordingly. Each of the parts was scanned with a "short track" exposure strategy, as well for the normal scanning as the post scanning step. Figure 22 shows the measured stress distributions for the 50 and 100 per cent post scanning levels, compared to the case without post scanning. It can clearly be seen that the 50 per cent post scanning level reduces the tensile stress in the upper zone of the part (from 120 ± 7 to 84 ± 11 MPa). Scanning each layer twice with the normal scanning parameters (100 per cent) does not reduce the residual stresses inside the part; the already solidified layer is simply remelted partially and the same residual stress distribution remains. The stress reducing effect of heating the underlying layers could result in a reduction of stress levels, but it is cancelled out by the TGM mechanism that introduces new stress inside the part.

X-ray diffraction experiments

The Crack compliance method that was used in the experiments, offered the possibility to measure the residual stress trough the thickness of the test samples, unlike more traditional XRD and hole drilling stress measurement methods. Alas, the Crack compliance method fails to measure the stress at the part surface very accurately,

Figure 22 Measured stress distributions for different post-scanning parameters

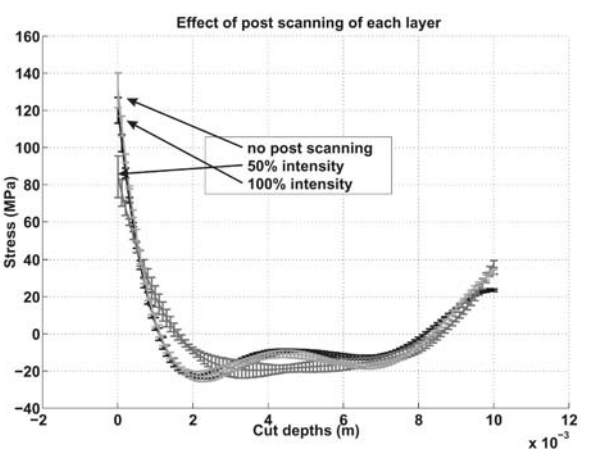

because of several reasons, some of which were already mentioned before:

- The first useful data point is the strain value recorded at the first cut depth. Therefore, the stress at the part surface is already an extrapolation of the calculated stress profile.
- The first few stress readings are rather small (less than 5 μm strain), and the uncertainty on these readings is therefore relatively large, resulting in a large stress uncertainty near the upper surface.
- The top face strain readings are very sensitive to the exact distance between the gauge and the edge of the cut. A slight positioning error of the top face gauge results in a large variation in the top face strains, causing erroneous results near the surface.

To cope with the large uncertainty of the stress readings near the surface, additional XRD tests were performed on several SLM samples. Due so practical size limitations, the SLM samples tested with the Crack compliance method, could not be tested using XRD, so a different set of test samples was produced.

The X-ray diffraction stress measurements were performed on a Siemens D500 diffractometer. The diffraction peak of the 316L stainless steel material at a 2θ angle of 147° was used to measure the peak shift.

Sample preparation

A first X-ray diffraction experiment on a untreated SLM sample, resulted in a stress level of 12 ± 7 MPa. This unrealistically low value was caused by the roughness of the top surface. Since the X-rays penetrate the material only to a depth of about 30 μm, large roughness values prohibit a correct stress measurement.

To cope with this problem, an EDM finishing cut was used to remove the peaks from the surface. However, the EDM operation itself introduces large tensile stresses in a $\pm$ 40 μm thick zone below the surface (Kruth and Bleys, 2000), which deteriorates the measurement result. Therefore, the thermally influenced layer from the EDM operation was removed by chemically etching a small top layer from the samples[2].

Figure 23 shows the sample preparation steps schematically. Figure 24 shows the results of three different XRD measurement on a stress free dummy sample that was used to check the influence of the sample preparation steps.

The first XRD measurement indicates a low but non-zero stress value in X direction (the Y direction was not measured). The non-zero value was probably caused by the presence of a small oxide layer resulting from the heat treatment. Next, the dummy sample was cut with wire-EDM on a finishing regime. The second XRD measurement reveals very large stress values X and Y direction. There is no significant difference between the direction of the cut and the direction of the wire. The third XRD measurement indicates the stress values after the etching step. It is clear that the small thermally influence layer of the EDM process is removed

Figure 23 XRD sample preparation steps

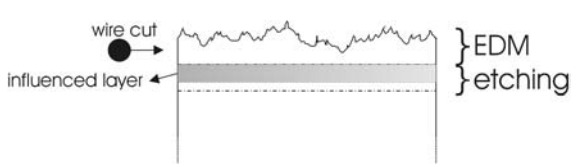

Figure 24 XRD result with stress free dummy sample

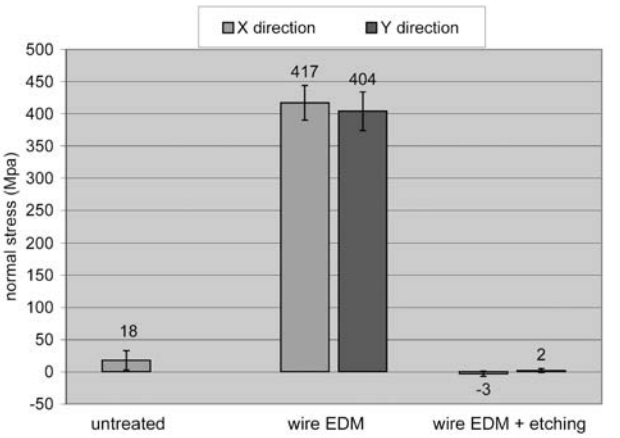

in the etching step and a zero stress value is measured indeed in X and Y direction.

Owing to the removal of the upper layer, the stress values that are measured are not any more the values at the upper layer of the SLM part. However, the total removed thickness of about 120 μm is small enough compared to the total height of the XRD test samples (10.5 mm) to consider them as the top layer stress values.

The influence of the base plate removal step is shown in Figure 25. The sample that was tested was exposed with a random sector exposure. Thus, the stresses are equally large in X and Y direction. The same sample was then cut from its base plate and was measured again. It is clear that the base plate removal yields a large reduction of the stress levels.

The influence of the number of layers was investigated by testing a series of three samples, having a height of 2.5, 5 and 10 mm, respectively. The base plate was removed with all samples. All three samples were scanned without dividing the surface in sectors, to check the influence of the scanning direction on the residual stresses. Figure 26 shows the axis orientation and the exposure strategy that was used. From Figure 27 it can clearly be seen that the sample height has a large influence on the residual stress level, as expected from the theoretical model. Furthermore, Figure 27 shows the influence of the scanning direction on the residual stresses;

Figure 25 Influence of base plate removal

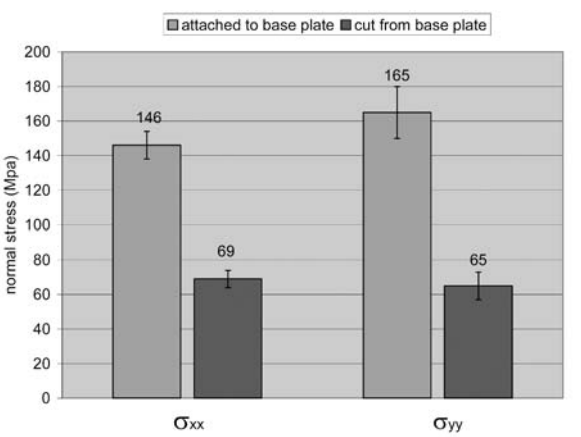

Figure 26 Exposure strategy and axis orientation

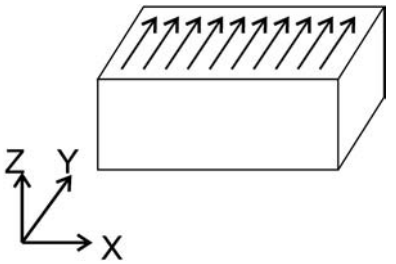

Figure 27 Influence of the sample height

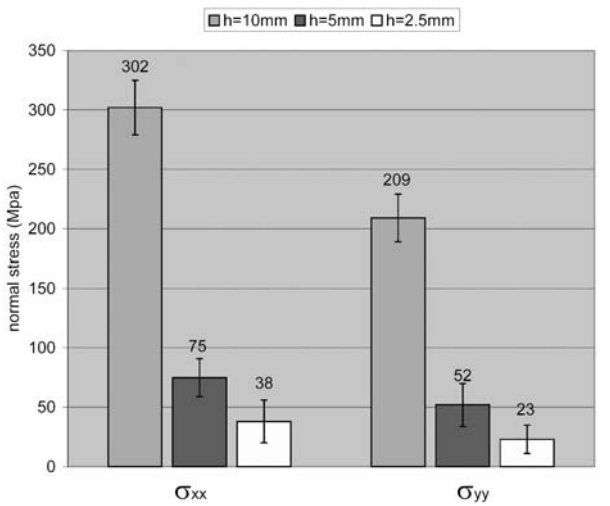

the stresses perpendicular to the scanning direction are significantly larger than the stresses along the scanning direction. This result corresponds to the Crack compliance experiments.

Since residual stresses arise from temperature gradients, heating up the build platform can reduce the stress levels present in the parts (Over, 2003),(Vasinonta *et al.*, 2000). To validate this assumption the build platform was heated up to 200°C. Figure 28 shows the effect of the raised based plate temperature. It is clear that the stresses are reduced by the base plate heating. However, the stress reduction is rather poor. It can be expected that a higher base plate heating temperature will result in a greater stress reduction. Like Figure 27, Figure 28 also clearly indicates the influence of the scanning direction.

In general, there is a good qualitative agreement between the theoretical model, the Crack compliance experiments and the XRD tests. However, a quantitative comparison is not easy, because of several reasons:

- The theoretical model calculates the stresses resulting from the shrinkage of the added molten layers. It does not include the TGM, which induces extra residual stresses.
- The sample geometry of the Crack compliance test samples and the XRD samples was different, due to practical reasons.
- The Crack compliance test samples and the first batch of XRD test samples, used non optimized scanning parameters, which appeared to contain a rather high degree of porosity. This resulted in stress values much lower than in the case of full density, since the stress equals zero at each porosity border. The XRD samples from Figures 27 and 28 were build with optimized scanning parameters, yielding nearly 100 per cent density and having much higher stress values.

Figure 28 Influence of base plate heating

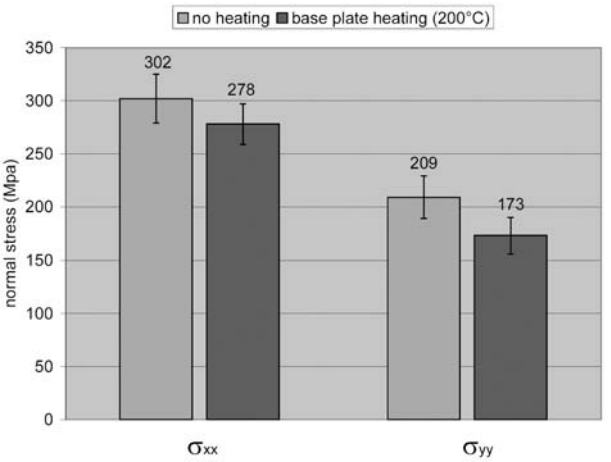

Conclusions

This paper presented a theoretical and experimental investigation on residual stresses in SLS and SLM. A simple theoretical model could predict the basic shape of the residual stress profile of a basic rectangular geometry. Two experimental methods -the Crack Compliance Method and an X-ray diffraction method -were used to validate the theoretical predictions and to find a qualitative and quantitative estimation of the residual stresses.

From the theoretical model and the experiments, some important conclusions can be derived:

- A distinction should be made between parts that remain connected to their base plate and parts that are removed afterwards. In general, parts that stay connected to the baseplate contain very high stress levels, in the range of the material's yield strength. Parts that are removed from the base plate, contain much lower stress levels, but they suffer from deformation during part removal.
- The basic residual stress distribution in the *Z* direction for a part removed from its base plate, consists of a zone of tensile stresses just below the upper surface, followed by a large zone of compressive stress, to end again with a tensile stress zone at the bottom. The magnitude of the stresses depends amongst others on the part height and the stiffness and height of the base plate.
- The exposure strategy that is being used to fuse the powder layers, has a large influence on the residual stress levels being developed. In general, the stresses are larger perpendicular to the scan direction than along the scan direction. A subdivision of the surface in smaller parts results in a lower maximum stress value and in equally large stresses in *X* and *Y* direction.

- It is possible to reduce the stress level by applying a heat treatment using the laser source. However, no drastic reductions could be obtained in this investigation.
- Heating of the substrate plate results in a reduction of the residual stress level, since temperature gradients are reduced.

Notes

1. The calculations were performed using the Abaqus FEM package.
2. A mixture of HCl and HNO_3 was used to remove a top layer of $\pm 80\ \mu$m thickness from the top surface.

References

Aggarangsi, P. and Beuth, J. (2003), "Melt pool size and stress control for laser-based deposition near a free edge", *Proceedings of the Solid Freeform Fabrication Symposium*, pp. 196-207.

Kruth, J. and Bleys, P. (2000), "Measuring residual stress caused by wire EDM of tool steel", *International Journal of Electrical Machining*, Vol. 5, pp. 23-8.

Kruth, J., Froyen, L., Rombouts, M., van Vaerenbergh, J. and Mercelis, P. (2003), "New ferro powder for selective laser sintering of dense parts", *Annals of the CIRP*, pp. 139-42.

Kruth, J., Mercelis, P., Froyen, L. and Rombouts, M. (2004), "Binding mechanisms in selective laser sintering and selective laser melting", *Proceedings of the Solid Freeform Fabrication Symposium*, pp. 44-59.

Nowell, D., Hills, D. and Tochilin, S. (2000), "Use of the crack compliance method for the measurement of residual stress", *Proceedings of the 6th International Conference on Residual Stresses*, Vol. 2, pp. 845-52.

Over, C. (2003), "Generative Fertigung von Bauteilen aus Werkzeugstahl X38CrMoV5-1 und Titan TiAl6V4 mit Selective Laser Melting", PhD thesis, RWTH Aachen.

Prime, M. (1999), "Residual stress measurement by seccessive extension of a slot: the crack compliance method", *Applied Machanics Reviews*, Vol. 52 No. 2, pp. 75-96.

Schindler, H. (2000), "Residuals stress measurements in cracked components: capabilities and limitations of the cut compliance method", *Materials Science Forum*, Vol. 347-349, pp. 150-5.

Vasinonta, A., Beuth, J. and Griffith, M. (2000), "Process maps for controlling residual stress and melt pool size in laser-based sff processes", *Proceedings of the Solid Freeform Fabrication Symposium*, pp. 200-8.

Withers, P. and Bhadeshia, H. (2001), "Residual stress, part 2 -nature and origin", *Materials Science and Technology*, Vol. 17, pp. 366-75.

About the authors

Peter Mercelis obtained a MSc degree in Mechanical Engineering -Mechatronics at the University of Leuven and is currently working as a PhD candidate at the department of Mechanical Engineering at the University of Leuven. He is part of the research group on production processes. His research focuses mainly on process monitoring and control in Selective Laser Sintering and Selective Laser Melting of metal powders. Peter Mercelis is the corresponding author and can be contacted at: peter.mercelis@mech.kuleuven.ac.be; web site: http://people.mech.kuleuven.ac.be/ ~ pmerceli/

Jean-Pierre Kruth is Full Professor at the University of Leuven, (KU Leuven), Belgium, where he is responsible for Production Engineering. His main research activities are: CAD/CAM/CAPP, production processes, metal cutting, non-traditional machining (EDM, laser machining, ...), Rapid Prototyping and Manufacturing, dimensional metrology, quality control, reverse engineering. He is Active Member of CIRP, Fellow of SME, Honorary member Romanian Society of Mech. Eng., Member BSMEE, Member IMEKO/ BEMEKO, Member K.VIV and founding board member of the companies MATERIALISE N.V. (1997), METRIS N.V., MIH N.V. Email: jean-pierre.kruth@mech.kuleuven.be; website: www.mech.kuleuven.be/pma/